Coulomb and radiation screening in photoconductive terahertz sources

Dae Sin Kim and D. S. Citrin

Citation: Appl. Phys. Lett. **88**, 161117 (2006); doi: 10.1063/1.2196480
View online: http://dx.doi.org/10.1063/1.2196480
View Table of Contents: http://apl.aip.org/resource/1/APPLAB/v88/i16
Published by the American Institute of Physics.

Coulomb and radiation screening in photoconductive terahertz sources

Dae Sin Kim[a] and D. S. Citrin
School of Electrical and Computer Engineering, Georgia Institute of Technology, Atlanta, Georgia 30332-0250 and Georgia Tech Lorraine, 2-3, rue Marconi, Metz Technopole 57070 Metz, France

(Received 14 November 2005; accepted 11 March 2006; published online 20 April 2006)

We distinguish the screening contributions due to the Coulomb and radiation parts of the electromagnetic field subsequent to the ultrafast photogeneration of electron-hole pairs in photoconductive GaAs terahertz (THz) sources. We employ the Monte Carlo method self-consistently including the Maxwell equations to study the effects of the excitation-spot size and excitation level on the emitted THz radiation, and find for a range of reasonable excitation levels an excitation-spot diameter of $\sim 100\ \mu$m as the crossover point beyond which radiation effects dominate screening. © *2006 American Institute of Physics*. [DOI: 10.1063/1.2196480]

Ultrafast broadband terahertz (THz) transients generated by femtosecond optical pulses incident on biased photoconductors are commonly employed for THz sources. A great effort has been made to improve the performance due to their typically low THz output power (a few hundred nW) and optical-to-THz conversion efficiency ($<0.01\%$), usually using large excitation-aperture emitters because of the relatively small photocarrier screening of the bias field.[1–3] To enable the development of compact THz systems with high radiation power, however, we need to consider the overall efficiency with an eye to the limitations due to screening[4] related to excitation-spot size. One of the unsolved issues in the generation of THz radiation from photoconductors with relative small excitation-apertures is to clarify the relative roles played by the direct Coulomb screening of the bias field by the photogenerated carriers and the radiation screening due to the back action of the THz field on the device itself.[5] On the one hand, for a large excitation-aperture, where the excitation-spot size well exceeds the center wavelength of the emitted THz transient, radiation effects can be derived from simple electromagnetic boundary conditions.[1,2] On the other hand, when the spot size is considerably smaller than the center wavelength of the THz radiation, the boundary conditions cannot be used because the electric fields are not uniform over the excitation-aperture boundary. This approach is therefore invalid for photoconductive switches with relatively small gap, which produce highly divergent radiation. Thus, to consider the back action of the radiation field on the dynamics of the carriers as well as that due to the static Coulomb field arising from the electron-hole pairs, we report in this letter an approach using the retarded electromagnetic field from moving groups of charges.[6–8] We find that if the electromagnetic propagation time across the emitter is longer than the duration of the generated electromagnetic transients (~ 1 ps), then the relative importance of Coulomb and radiation screening clearly depends on the excitation-spot size. Moreover, we predict an enhancement of the optical-to-THz conversion efficiency with increasing excitation-aperture for a given optical excitation power compared with what would be expected based on screening.

When a photoconductor is excited by high peak-fluence optical pulses, the accelerated motion of the electrons (and to a lesser extent, holes) by the bias field results in the emission of THz radiation, but at the same time, as the carriers undergo their spatial dynamics in the bias field, they partially screen out the bias. The origins of the screening consist of the radiation field and the space-charge field, which contribute to the collapse of the total electric field acting on the carriers at high carrier density.[1,9] To explore the screening associated with the photoexcited carriers, we divide the carrier densities spatially into groups of moving charges, and from these, compute the emitted electric fields that then act back on the various groups of charges. The electric field due to a point charge q moving with velocity $\mathbf{v}$ and acceleration $\mathbf{a}$ is[8]

$$\mathbf{E} = \frac{q}{4\pi\varepsilon}\left(\frac{1}{|1-\hat{R}\cdot\mathbf{v}/c|^3}\left\{\frac{(1-v^2/c^2)(\hat{R}-\mathbf{v}/c)}{R^2} + \frac{\hat{R}\times[(\hat{R}-\mathbf{v}/c)\times\mathbf{a}]}{c^2 R}\right\}\right)_{t_r}, \tag{1}$$

where ε is the permittivity, c is the speed of light in photoconductor (background dielectric), and $\mathbf{R}$ is the position vector directed from charge q to the point of observation. $\mathbf{R}$, $\mathbf{v}$, and $\mathbf{a}$ are evaluated at the retarded time $t_r = t - R/c$ where t is the present time for which $\mathbf{E}$ is evaluated. The magnitude and direction of the electric field at each location are the sum of the electric-field vectors for each individual charge. To distinguish the Coulomb and radiation components of the field, if the maximum drift velocity of the photoexcited carriers is much less than the speed of light, $v/c \ll 1$, the electric field of Eq. (1) can be conveniently split into two components: the Coulomb field, $\mathbf{E}_c$, and the radiation field $\mathbf{E}_r$,[8,10]

$$\mathbf{E} \cong \mathbf{E}_c + \mathbf{E}_r = \frac{q}{4\pi\varepsilon}\left(\frac{\hat{R}}{R^2}\right)_{t_r} + \frac{q}{4\pi\varepsilon c^2}\left(\frac{\hat{R}\times(\hat{R}\times\mathbf{a})}{R}\right)_{t_r}. \tag{2}$$

When the charge is stationary ($\mathbf{v}=0$, $\mathbf{a}=0$), we have only the Coulomb field $\mathbf{E}_c$ while the radiation field $\mathbf{E}_r$ is expected to dominate for large values of the acceleration. To include numerically even small effects of the drift velocity in $\mathbf{E}_r$ or $\mathbf{E}_c$, we can subtract $\mathbf{E}_c$ or $\mathbf{E}_r$ from the electric field E in Eq. (1), respectively.[11] To obtain the transport properties ($\mathbf{R}$, $\mathbf{v}$, and $\mathbf{a}$) of the photoexcited carriers, we solved the Boltzmann equa-

[a]Electronic mail: dskim@ece.gatech.edu

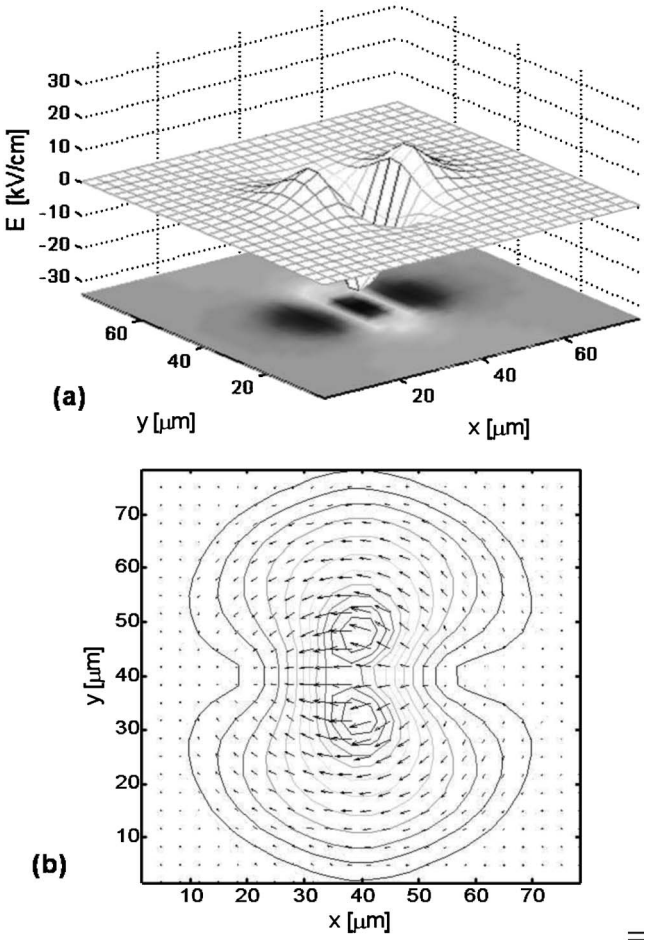

FIG. 1. (a) The Coulomb screening field induced by the space charge. (b) The direction of radiation screening field caused by accelerating charges.

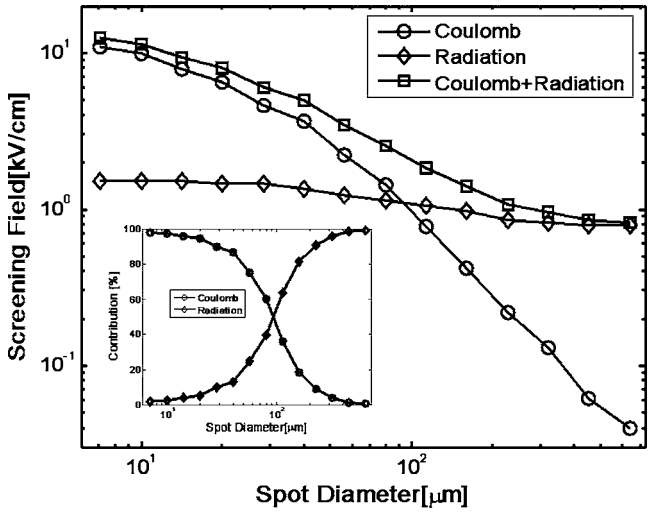

FIG. 2. Coulomb and radiation screening field vs excitation-spot diameter for a given carrier density 10^{17} cm^{-3}. Inset: Contribution of the Coulomb and radiation field to the screening field vs excitation-spot diameter.

tions employing the Monte Carlo method[12–15] We include the three nonparabolic valleys Γ, L, and X within the conduction band and warped heavy- and light-hole bands.[16–18]

We consider a GaAs-based photoconductive source laterally biased at 40 kV/cm in the x direction excited by a 75-fs full width at half maximum (FWHM) optical pulse spectrally centered at 800 nm with a repetition rate of 76 MHz. Patterned on top of the device are assumed to be two infinitely long parallel electrodes, between which is the photoconductive gap four times the excitation-spot diameter. Various excitation-spot sizes and levels incident upon this gap were simulated. The optical excitation acts as a carrier source within the Monte Carlo simulation; the carrier source terms are taken as Gaussian both temporally and spatially to match the optical excitation pulse. We give results in Fig. 1 for the Coulomb field profiles and the radiation field induced by accelerating carriers after laser excitation with a 20-μm FWHM spot diameter for a peak carrier density of 10^{17} cm^{-3}. Since the net positive and negative space charges develop as the electrons and holes drift in opposite direction, the electric field induced by this space charge screens the bias field as shown in Fig. 1(a). The directional characteristics of the radiation field depend upon the relative orientation of the velocity and the acceleration, as shown in Eq. (1). Thus, the electric field induced by the accelerating carriers is also in the direction opposite to the bias field as shown in Fig. 1(b). These Coulomb and radiation fields effectively collapse the bias field driving the carriers and results in the saturation of THz output field strength. The Coulomb screening field near the spot edges is weaker than at the center of the Gaussian laser spot as shown in Fig. 1(a), since the carrier density decreases toward the edges.[9,19] In Fig. 1(b), we can see that the radiation field near the edges of the spot away from its center in the y direction is stronger than anywhere else since the carriers near these edges move faster than those elsewhere because of the weak Coulomb screening field. The peak points of the radiation screening field move to the anode due to the high mobility of the electrons comparing to the holes.

First, to distinguish between the Coulomb contribution that produces space-charge screening and the radiation contribution caused by the acceleration of carriers as a function of excitation-aperture size, we maintain the peak excited carrier densities 10^{17} cm^{-3}. (Thus the total optical pulse energy varies with spot size.) Figure 2 shows the screening field (the x component of the retarded field) as a function of spot diameter maintaining a given carrier density by adjusting the incident optical power. As the excitation-spot size increases, the overlap of the photoexcited electron and holes also increases. Thus, relatively small net positive and negative space charges develop, and the distance between them increases. One can see the Coulomb screening decrease as the excitation-spot diameter increases. Meanwhile, for the radiation screening, although the excitation-aperture size increases, the radiation field remains essentially constant with excitation-spot size due to the same carrier density. The contributions of Coulomb and radiation screening are shown in the inset of Fig. 2. One sees the Coulomb screening field is dominant up to an excitation-spot size of $\sim$100 μm FWHM, but for larger spot size, the radiation field dominates.

In the typical experiment one has fixed optical power, but can vary the spot size by means of focusing optics. In this case, as the excitation-spot size increases, the Coulomb screening field decreases rapidly as shown in Fig. 3 (compare with Fig. 2) because the distance between the carriers increases due to the decrease of carrier density. In addition, as the carrier density becomes sparse, the carrier numbers contributing the Coulomb and radiation screening field decrease. As a result, the radiation screening field also decreases as the excitation-aperture size increases, as shown in Fig. 3. The

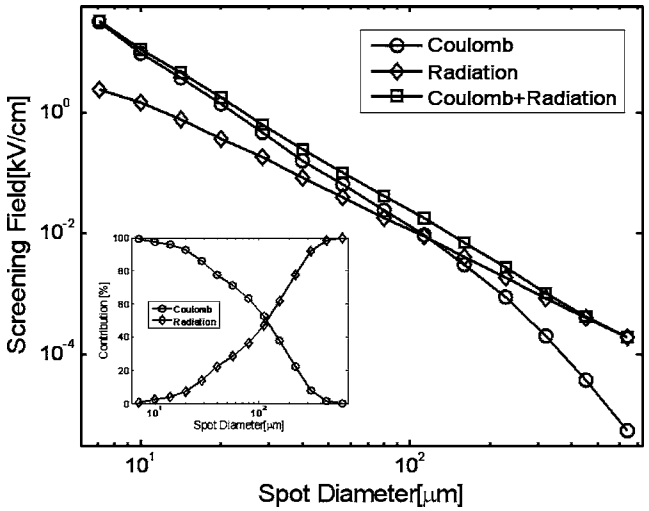

FIG. 3. Coulomb and radiation screening field vs excitation-spot diameter for a given optical excitation power 5 mW. Inset: Contribution of the Coulomb and radiation field to the screening field vs excitation-spot diameter.

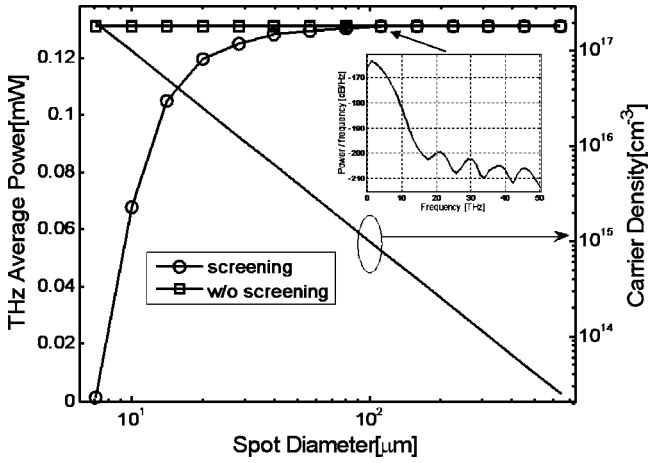

FIG. 4. The THz average radiation power as a function of excitation-spot diameter for a given optical power 5 mW. Inset: THz power spectral density estimate at a 100 μm FWHM excitation-spot diameter.

contributions of Coulomb and radiation screening in this case are shown in the inset of Fig. 3. One sees similar contributions to the screening field in the inset of Fig. 2 except for the gradual slope resulting from the decrease of both of the Coulomb and radiation fields at the same time.

In the absence of screening, as optical excitation increases, the THz radiation power also increases due to the quadratic dependence of the THz radiation power on the number of charges contributing,[8,10]

$$P \cong \frac{1}{6\pi\varepsilon_0}\frac{N^2 q_{sc}^2 \langle a \rangle^2}{c^3}, \tag{3}$$

where N is the number of carriers in the ensemble, q_{sc} is the supercharge representing a subpopulation of the carriers in the real device, and $\langle a \rangle$ is the retarded ensemble average of the acceleration. The THz power also originates from carrier acceleration by the bias field since the THz power is proportional to the square of the acceleration, as shown in Eq. (3). Thus for a given excitation level, if we maintain the external bias field by reducing the screening as we increase the excitation-aperture size as in Fig. 3, we obtain optimal conversion efficiency from optical to THz radiation as shown in Fig. 4. One sees the enhancement of the optical-to-THz conversion efficiency defined by the ratio of average THz radiation power and the optical excitation power (5 mW) from 0.024% to 2.6% as the excitation-spot diameter increases from 7 μm FWHM (THz average power: 1.24 μW—within an order of magnitude of the experimental result in Ref. 4) to more than 100 μm FWHM (THz average power, 0.13 mW). We obtain the THz average power from power spectral density (PSD) like that in the inset of Fig. 4 by the integration over the frequency range of PSD (Ref. 20).

To conclude, we have distinguished two contributions to the THz radiation associated with the Coulomb and radiation fields acting back on the carrier dynamics within the first picosecond. In this way, we have identified which of the Coulomb and radiation fields is dominant with varying excitation-aperture sizes, and have found that these screening effects may be the main factor underlying radiation power saturation. For a given optical excitation power, we predict that the enhancement of the optical to THz conversion efficiency with a broaden excitation-aperture is possible. For a given optical excitation power (5 mW in this letter), the conversion efficiency with excitation-spot diameter more than 100 μm FWHM is enhanced by a factor of 100 compared with 7 μm FWHM excitation-spot diameter.

This work was supported in part by the National Science Foundation by ECS 0523923 and DMR 0305524.

[1] J. T. Darrow, X.-C. Zhang, D. H. Auston, and J. D. Morse, IEEE J. Quantum Electron. **28**, 1607 (1992).
[2] P. K. Benicewicz, J. P. Roberts, and A. J. Taylor, J. Opt. Soc. Am. B **11**, 2533 (1994).
[3] G. Rodriguez and A. J. Taylor, Opt. Lett. **21**, 1046 (1996).
[4] J. H. Kim, A. Polley, and S. E. Ralph, Opt. Lett. **30**, 2490 (2005).
[5] B. B. Hu, E. A. De Souza, W. H. Knox, J. E. Cunningham, and M. C. Nuss, Phys. Rev. Lett. **74**, 1689 (1995).
[6] G. S. Smith, Am. J. Phys. **69**, 288 (2000).
[7] J. D. Jackson, *Classical Electrodynamics*, 3rd ed. (Wiley, New York, 1999), pp. 661–665.
[8] G. S. Smith, *An Introduction to Classical Electromagnetic Radiation* (Cambridge University Press, Cambridge, 1990), pp. 358–378.
[9] M. Bieler, G. Hein, K. Pierz, and U. Siegner, Appl. Phys. Lett. **77**, 1002 (2000).
[10] W. E. Baylis, *Electrodynamics: A Modern Geometric Approach* (Birkhauser, Boston, 1999), pp. 248–266.
[11] A. R. Janah, T. Padmanabhan, and T. P. Singh, Am. J. Phys. **56**, 1036 (1988).
[12] C. Jacoboni and L. Reggiani, Rev. Mod. Phys. **55**, 645 (1983).
[13] W. Fawcett, A. D. Boardman, and S. Swain, J. Phys. Chem. Solids **31**, 1963 (1970).
[14] J. G. Rush and W. Fawcett, J. Appl. Phys. **41**, 3843 (1970).
[15] M. A. Osman and D. K. Ferry, Phys. Rev. B **36**, 6018 (1987).
[16] N. Nintunze and M. A. Osman, Semicond. Sci. Technol. **10**, 11 (1995).
[17] T. Brudevoll, T. A. Fjeldly, J. Baek, and M. S. Shur, J. Appl. Phys. **67**, 7373 (1990).
[18] M. T. Portella, J.-Y. Bigot, R. W. Schoenlein, J. E. Cunningham, and C. B. Shank, Appl. Phys. Lett. **60**, 2123 (1992).
[19] D. S. Kim and D. S. Citrin, Appl. Phys. Lett. **87**, 61108 (2005).
[20] J. G. Proakis, D. G. Manolakis and *Digital Signal Processing Principles, Algorithms, and Applications*, 3rd ed. (Prentice-Hall, Englewood Cliffs, NJ, 1996), pp. 896–920.